[Short title + Author Name - P&H title] 17 (2024) 105450

Contents lists available at ScienceDirect

Arabian Journal of Chemistry

journal homepage: www.ksu.edu.sa

Fabrication of highly efficient nanofiltration membranes decorated with praseodymium based triamino-functionalized MCM-41 for desalination and micropollutants removal

Shehzada Muhammad Sajid Jillani [a], Abdul Waheed [a,*], Umair Baig [a,*], Isam H. Aljundi [a,b]

[a] Interdisciplinary Research Center for Membranes and Water Security, King Fahd University of Petroleum and Minerals, Dhahran 31261, Saudi Arabia
[b] Chemical Engineering Department, King Fahd University of Petroleum & Minerals (KFUPM), Dhahran 31261, Saudi Arabia

ARTICLE INFO

Keywords:
In-situ synthesis
Interfacial polymerization
MCM-41 zeolites
Micropollutants
Praseodymium oxide

ABSTRACT

The nanofiltration membranes with a stable decoration of inorganic fillers such as zeolites are desperately required for enhancing the desalination performance of the membranes and hence three nanofiltration membranes were fabricated by decorating the membranes with praseodymium-based triamino-functionalized MCM-41 (Pr-$(NH)_2NH_2$-MCM-41). The membranes were applied for the removal of emerging pharmaceutically active micropollutants from water. The Pr-$(NH)_2NH_2$-MCM-41 was synthesized by using an *in-situ* approach where praseodymium oxide was chemically decorated in the framework of MCM-41 followed by simultaneous amine functionalization using N1-(3-Trimethoxysilylpropyl)diethylenetriamine (TMSPTA). A thorough characterization of the synthesized Pr-$(NH)_2NH_2$-MCM-41 was carried out by using HR-TEM, SEM, WCA, XRD, FTIR, BET, elemental and mapping analysis. Three different concentrations of synthesized Pr-$(NH)_2NH_2$-MCM-41 were decorated in the membrane active layer through interfacial polymerization in the presence of an aqueous tetra-amine solution and using terephthaloyl chloride as an organic crosslinker. Subsequently, the fabricated membranes were used for desalinating saline feed containing divalent ($CaCl_2$, $MgCl_2$, Na_2SO_4, $MgSO_4$) and monovalent (NaCl) ions. The rejection of salts by PA/0.05-Pr-MCM@PSU/PET membrane was found to be the highest among all the fabricated membranes which were found to be 98 %, 96 %, 95 %, 87 %, and 82 % for $CaCl_2$, $MgCl_2$, $MgSO_4$, Na_2SO_4 and NaCl, respectively. The permeate flux was found to be dependent on the applied feed pressure which was found to be 56 L m^{-2} h^{-1} (LMH) at 25 bar for PA/0.050-Pr-MCM@PSU/PET membrane. The rejection performance of the membranes was also evaluated by using different well-known pharmaceuticals (Caffeine, Sulfamethoxazole, Amitriptyline, and Loperamide) as micropollutants in the feed. All the pharmaceutical drugs were found to be highly rejected > 96 % by PA/0.5-Pr-MCM-41@PSU/PET membrane followed by PA/0.025-Pr-MCM-41@PSU/PET membrane. Therefore, the current approach of synthesizing functionalized zeolites is quite effective and efficient for the stable decoration of inorganic fillers in the membrane active layer and should be extended to other zeolites such as zeolites with antimicrobial potential.

1. Introduction

The quest for clean water is increasing at an alarming rate due to the demand for clean water for several industrial processes (Aldossari, 2023; Chowdhary et al., 2020; Schleifer, 2017). In addition, clean water is also required for numerous domestic activities for maintaining day-to-day chores of life. Similar to increasing clean water demand, several newly emerging strict environmental regulations put more constraints on the treatment and disposal of both domestic and industrial wastewater (Du et al., 2021; Gassem, 2021). The wastewater generated from industries has a variety of pollutants such as dyes from the textile industry (Dutta et al., 2021), drugs and pharmaceuticals from hospital discharge (Waheed et al., 2023b), saline and oily wastewater generated in the oil and gas industry (Baig et al., 2022; Yu et al., 2017). Hence, the wastewater from different industries must be treated efficiently to recover clean water which can be used as and when needed.

Quite a few water treatment methodologies and techniques are known to date which include screening, filtration, dissolved air

Peer review under responsibility of King Saud University.
* Corresponding authors.
E-mail addresses: abdul.waheed@kfupm.edu.sa (A. Waheed), umairbaig@kfupm.edu.sa (U. Baig).

https://doi.org/10.1016/j.arabjc.2023.105450
Received 18 September 2023; Accepted 8 November 2023
Available online 10 November 2023

floatation, and sedimentation (Chai et al., 2021; Saravanan et al., 2021; Yadav et al., 2022). In addition, chemical-based wastewater treatment methods such as flocculation, adsorption, chemisorption, ozonation, oxidative and reductive degradation of pollutants, precipitation, and ion exchange (Qasem et al., 2021; Wang et al., 2022, 2021, 2020). Although the above-mentioned methodologies have proved to be viable for treating large quantities of wastewater, most of these technologies are pretreatment steps that do not generate considerably clean water. In addition, these methodologies have certain disadvantages such as the generation of huge quantities of sludge which require proper disposal and degradation(Kacprzak et al., 2017). Similarly, high energy costs and regeneration of materials such as ion-exchange resins are the major challenges faced during the operation of these methodologies. In comparison, membrane-based separation is advantageous because of its certain salient features such as ease of availability for different types of feeds, ease of tuneability for matching the desired requirements, little footprint compared to large land areas required for air floatation, high permeate flux with clean water as output, rejection of a variety of species such as divalent and monovalent salts, dyes, drugs, pharmaceutical compounds and even the by-products generated during chemical degradation of pollutants (Ahmad et al., 2020; Dharupaneedi et al., 2019; Saxena et al., 2009). Hence, many efforts in literature have been focused on developing novel and efficient membranes with enhanced performance in terms of rejection and permeate flux (Alsohaimi et al., 2023; El-Sayed et al., 2023).

Several techniques have been used in literature for enhancing the performance of membranes such as increasing the volume of permeate flux, increasing the % rejection of salts, and antifouling behavior of membranes. To achieve enhanced nanofiltration performance of the membranes, researchers have used different approaches which include developing an interlayer between the ultrafiltration support and polyamide active layers of the thin film composite (TFC) membranes. In one such example, Jing-Jing Wang et. al. developed a nanofiltration membrane through interfacial polymerization (IP) between piperazine (PIP) and trimesoyl chloride (TMC) on a cellulose nanocrystal interlayer supported by microporous support. Due to the presence of cellulose nanocrystal interlayer, the membrane showed a flux of 204 L $m^{-2}h^{-1}$ (LMH) at 0.6 Mpa and Na_2SO_4 rejection of 97 % (Wang et al., 2017). The decoration of nanomaterials in the ultrafiltration support or active layers of the membranes has also been explored in the literature to enhance the performance of the membranes. In one such example, Lewis Yung et. al. fabricated a TFC membrane by incorporating two different ionic liquids (ILs) (with different molecular sizes) in the active layer of the membrane. The ILs were added to aqueous PIP solution which was crosslinked with TMC during IP. The IL with a smaller size of 1-butyl-3-methyl-imidazolium chloride (BMIC) led to an increase in salt rejection (99.1 % to 99.3 % of $MgSO_4$) with a decrease in permeate flux (32.5 LMH to 12.9 LMH). The larger-sized IL 1-octyl-3-methylimidazolium chloride (OMIC) showed an opposite effect to BMIC because the rejection of salts was decreased (99.1 % to 91.9 % of $MgSO_4$) with an increase in permeate flux (32.5 LMH to 60.3 LMH) of the membrane (Yung et al., 2010). Hence, the incorporation of a suitable additive in the membrane structure during IP would have a considerable impact on the performance of the membranes.

Similarly, several nanomaterials such as carbon nanotubes (CNTs), mesoporous silica, graphene oxide nanosheets, metal–organic frameworks (MOFs), and carbon organic frameworks (COFs) have been incorporated into the membranes. Among the nanomaterials, microporous or mesoporous such as MCM-41 has unique properties such as easy functionalization, homogenous hexagonal channel structure, large pore volume, large surface area, and excellent chemical and thermal stability. Due to these unique features, MCM-41 has found a wide range of applications such as drug delivery, extraction, adsorption, sensors, and support for catalysts. Due to its large surface area and porosity, MCM-41 has been used as a support with enhanced capacity for the loading of various catalysts and metal ions. Similarly, the large pore volume of MCM-41 also allows immobilization of organic ligands and metal ion complexes in the channels of MCM-41. Lanthanide metal ions have been incorporated into the channels and pores of MCM-41 for different applications. In one such example, a Schiff-base complex of lanthanum-catalyst was immobilized on MCM-41 as an efficient catalyst for the homoselective synthesis of substituted *1H*-tetrazole derivatives (Tahmasbi et al., 2022). Similarly, other lanthanides such as Praseodymium (Pr) have also been decorated in the MCM-41 framework. In one such example, X. Cao et. al. investigated a Pr-modified MCM-41 catalyst for the catalytic decomposition of methyl mercaptan (CH_3SH) (Cao et al., 2021). The catalytic ability of Pr was due to praseodymium oxide. Pr is a soft, silvery, metallic element that exists in two + 3 and + 4 general oxidation states (Zamani et al., 2008). The oxides of Pr have different phases which depend on the availability of oxygen in the ambient environment. Generally, praseodymium oxide exists in P_nO_{2n}-2 (n = 4, 7, 9, 10, 11, 12, etc.) homologous series with conversion from Pr_2O_3 to PrO_2 with a decrease in temperature and increase in oxygen content. The Pr_6O_{11} is considered a mixed oxide of $4PrO_2.Pr_2O_3$ contains oxygen vacancies and hence has a high hole and oxygen ion conductivity (Vshivkova et al., 2015). Due to the oxygen vacancies, the praseodymium oxide develops an affinity for water molecules which leads to the filling of oxygen vacancies in praseodymium oxide and results in protonated PrO_2 represented by $H_{0.334}PrO_2$. Therefore, the use of Pr in the framework of MCM-41 could potentially increase the performance of the membranes in terms of permeate flux while maintaining the rejection performance of the membranes. In addition, Lanthanides (Ln) also have huge coordination potential owing to their large atomic size and consequently large coordination numbers. Generally, the coordination number of lanthanide is usually eight or larger(Kanesato et al., 1996). Different types of additives that have been used for fabricating desalination membranes have been reviewed as shown in Table 1. Most of these additives are amino ($–NH_2$) functionalized for effective decoration in the membrane active layer via covalent bonding.

A careful design of the material structure can yield a promising material for desired applications. Previously, various doping materials and lanthanides have been decorated based on mere physical or ionic interaction which can be rendered unstable and washed out under high-pressure filtration experiments. Hence, the need of the day is to design a strategy where metal ions such as Ln can be covalently decorated in the MCM-41 framework to yield stable materials. The covalent decoration of Ln in MCM-41 enables the use of unique properties of Ln over an extended period and under high filtration pressure. Furthermore, the Ln covalently doped MCM-41 should also possess functional groups like amino groups ($–NH_2$) which can react during IP for decoration in the membrane active layer.

The current study is aimed at synthesizing an amino-functionalized zeolite for covalent decoration in the polyamide active layer of the membrane. Moreover, the zeolite was also decorated with transition metal Pr to further tune the features of the zeolites such as particle size and porosity for developing efficient desalination membranes. In an *in-situ* solvo-thermal synthesis of MCM-41, a Pr precursor namely Praseodymium methoxyethoxide (PrOMeEtO) was added to the reaction mixture resulting in covalent decoration of Pr in the MCM-41 framework. Similarly, N1-(3-Trimethoxy silylpropyl) diethylenetriamine (TMSPTA) was also added as a dual-purpose agent in the above reaction mixture. The TMSPTA becomes an integral part of MCM-41 where it serves as a ligand for complexation with Pr and on the other hand, TMSPTA confers several amino ($–NH_2$) groups to Pr decorated MCM-41. The resulting MCM-41 variant was named Pr-$(NH)_2NH_2$-MCM-41. The Pr-$(NH)_2NH_2$-MCM-41 was covalently decorated in the polyamide active layer of the TFC nanofiltration membrane during IP. Three different concentrations of Pr-$(NH)_2NH_2$-MCM-41 were decorated in polyamide active layers of the membranes. The synthesized Pr-$(NH)_2NH_2$-MCM-41 and fabricated membranes were thoroughly characterized for determining various structural features using different techniques which include SEM, TEM, water contact angle, AFM, ATR-

Table 1

Nanofiltration Membranes	Chemicals used for interfacial polymerization	Additives	Water Flux (L/ m^2.h)	Rejection of Salts (%)	Rejection of organic pollutants (%)	Ref.
PA/OMIC@PES	Piperazine (In aqueous phase) and Trimesoyl chloride (In organic Phase)	Ionic liquids; 1-butyl-3-methylimidazolium chloride (BMIC) and 1-octyl-3-methylimidazolium chloride (OMIC)	~ 50	~ 97.8 %	–	(Yung et al., 2010)
PEI/TPC-SiO_2 NPs/ PSf	Polyethyleneimine (In aqueous phase) and triphthaloyldichloride (In organic Phase)	SiO_2 nanoparticles	~ 13.3 L	–	~ 99 % Dyes	(Kebria et al., 2015)
PA/UIO-66-NH_2/ PD-SWCNT/PES	Piperazine (In aqueous phase) and Trimesoyl chloride (In organic Phase)	UIO-66-NH_2	46	~ 97.1 %	–	(Gong et al., 2020)
PA/Zeolite A/PS	m-phenylenediamine (In aqueous phase) and Trimesoyl chloride (In organic Phase)	Zeolite A nanoparticles	3.8 × 10^{12} m/ Pa.s	~ 94 %	–	(Jeong et al., 2007)
PA/UIO-66-NH_2/ H-PAN	Piperazine (In aqueous phase) and Trimesoyl chloride (In organic Phase)	UIO-66-NH_2	14.55	~ 99 %	–	(Liu et al., 2019)
Pr-MCM-41-NH_2-PA/PSf	2 % N,N-bis(2-aminoethyl)-1,3-propane diamine (Tetra-amine in aqueous phase) and 0.15 % Terephthaloyl chloride (In organic Phase)	Pr-MCM-41-NH_2	~ 56	~ 99 %	Pharmaceutical drugs ~ 97 %	This Work

FTIR, PXRD, and BET. The resulting membranes were applied for desalinating saline feed and removing several micropollutants from contaminated feed water.

2. Experimental

2.1. Materials

Polysulfone (Psf), N, N'-bis(3-aminopropyl)ethylenediamine (Tetra-amine, TA), Cetyltrimethylammonium bromide (CTAB), Tetraethyl orthosilicate (TEOS), Sodium hydroxide (NaOH), terephthalyol chloride (TPC), triethylamine (TEA), and were purchased from Sigma Aldrich, USA. The ethanol and hydrochloric acid (HCl) were purchased from Merck, Germany. Praseodymium methoxyethoxide (PrOMeEtO) and N1-(3-Trimethoxy silylpropyl) diethylenetriamine (TMSPTA) were purchased from Gelest USA. For the filtration test, different salts ($MgCl_2$, $CaCl_2$, $MgSO_4$, Na_2SO_4, NaCl) and pharmaceutically active compounds (Caffeine, Sulfamethoxazole, Amitriptyline, Loperamide) were also bought from Sigma. The chemicals utilized during the formation of mesoporous silica MCM-41 and membrane fabrication process are toxic but proper disposal is ensured.

The material was characterized using Powdered X-Ray Diffraction Ultima IV Rigaku, Transmission Electron Microscopy (JEOL, JEM2100F), Quantachrome: Autosorb (ASIQCU01000-6, USA), and scanning electron microscope (JEOL JSM6610LV, Japan). The material, active layer, and membranes were evaluated for the functional group vibrations using attenuated total reflectance-Fourier-transform infrared spectroscopy (Thermo, Smart iTR NICOLET iS10). The membranes' surface morphology, roughness, and hydrophilicity were characterized using a scanning electron microscope (JEOL JSM6610LV, Japan), Atomic force microscope (Agilent 550, Netherland), and Water contact angle (KRUSS DSA25) respectively. The solutions of salt and pharmaceutical were tested using a conductivity meter (Ultrameter II, Hanna) and JASCO V-750 UV–Vis spectrophotometer respectively.

2.2. Synthesis of Pr-$(NH)_2NH_2$-MCM-41

The in-situ metal bonding and amine-functionalized synthesis of MCM-41 was designed by learning from literature (Rahimi et al., 2021). The Pr-$(NH)_2NH_2$-MCM-41 was synthesized by dissolving 0.5 g of CTAB in 480 mL DI water and 7.0 mL of 2 M NaOH. This solution was stirred at 80 ℃ for 30 min. Later, TEOS (9.4 g) was added slowly to the stirring mixture and stirring was continued for an additional 30 min. Subsequently, triamine TMSPTA (20 % to TEOS molar ratio) and PrOMeEtO (20 % to TEOS molar ratio) were added respectively under continuous stirring for a further 1.5 h. The precipitated product was then centrifuged, washed multiple times with ethanol/HCl (100:1, V/V) mixture to remove CTAB, and dried at 90 ℃ in the oven. The current synthesis approach is defined as in-situ chemical bonding of Praseodymium oxide and triamine functionalized silane to mesoporous silica MCM-41 network and denoted as Pr-$(NH)_2NH_2$-MCM-41.

2.3. Membrane fabrication

Three different membranes were fabricated by altering the amount (0.025 % wt/v, 0.05 % wt/v, 0.1 % wt/v) of Pr-$(NH)_2NH_2$-MCM-41 in the active layers of membranes through interfacial polymerization (IP). Briefly, three aqueous amine solutions were prepared by dissolving 2 % wt/v of TA and 4 % TEA and different amounts (0.025, 0.05, and 0.1 %) of Pr-$(NH)_2NH_2$-MCM-41. The aqueous solution was thoroughly homogenized using a probe sonicator. The n-hexane solution was prepared by dissolving 0.2 % wt/v TPC crosslinker.

For the sake of fabricating ultrafiltration support of the nanofiltration membranes, polysulfone (Psf) was cast on polyester terephthalate (PET) using wet phase inversion methodology. Following wet phase inversion, the Psf/PET supports were dipped in SDS solution overnight. For IP, the Psf/PET supports were tapped onto the glass surface and dipped separately into three prepared aqueous amine solutions for 10 min while shaking in see saw direction. Upon amine impregnation and loading of Pr-$(NH)_2NH_2$-MCM-41, the Psf/PET supports were removed from aqueous amine solutions, and excess aqueous amine solution was removed using a rubber roller. Next, the amine-impregnated and Pr-$(NH)_2NH_2$-MCM-41 containing Psf/PET supports were dipped into an n-hexane solution for 1 min. The unreacted TPC was washed using excess n-hexane. Finally, for the sake of curing, the resultant membranes were kept inside the oven at 80 ℃ for 1 h. Hence prepared polyamide active layers were denoted as PA/0.025-Pr-MCM, PA/0.05-Pr-MCM, PA/0.025-Pr-MCM, and corresponding membranes to PA/0.025-Pr-MCM@PSU/PET, PA/0.05-Pr-MCM@PSU/PET, PA/0.1-Pr-MCM@PSU/PET respectively, based on material loading. A schematic representation of different steps of membrane fabrication by incorporating Pr-$(NH)_2NH_2$-MCM-41 in the active layer is shown in Fig. 1.

3. Results and discussion

The Pr-$(NH)_2NH_2$-MCM-41 was synthesized by using an in-situ simultaneous decoration of PrO and TMSPTA in the MCM-41

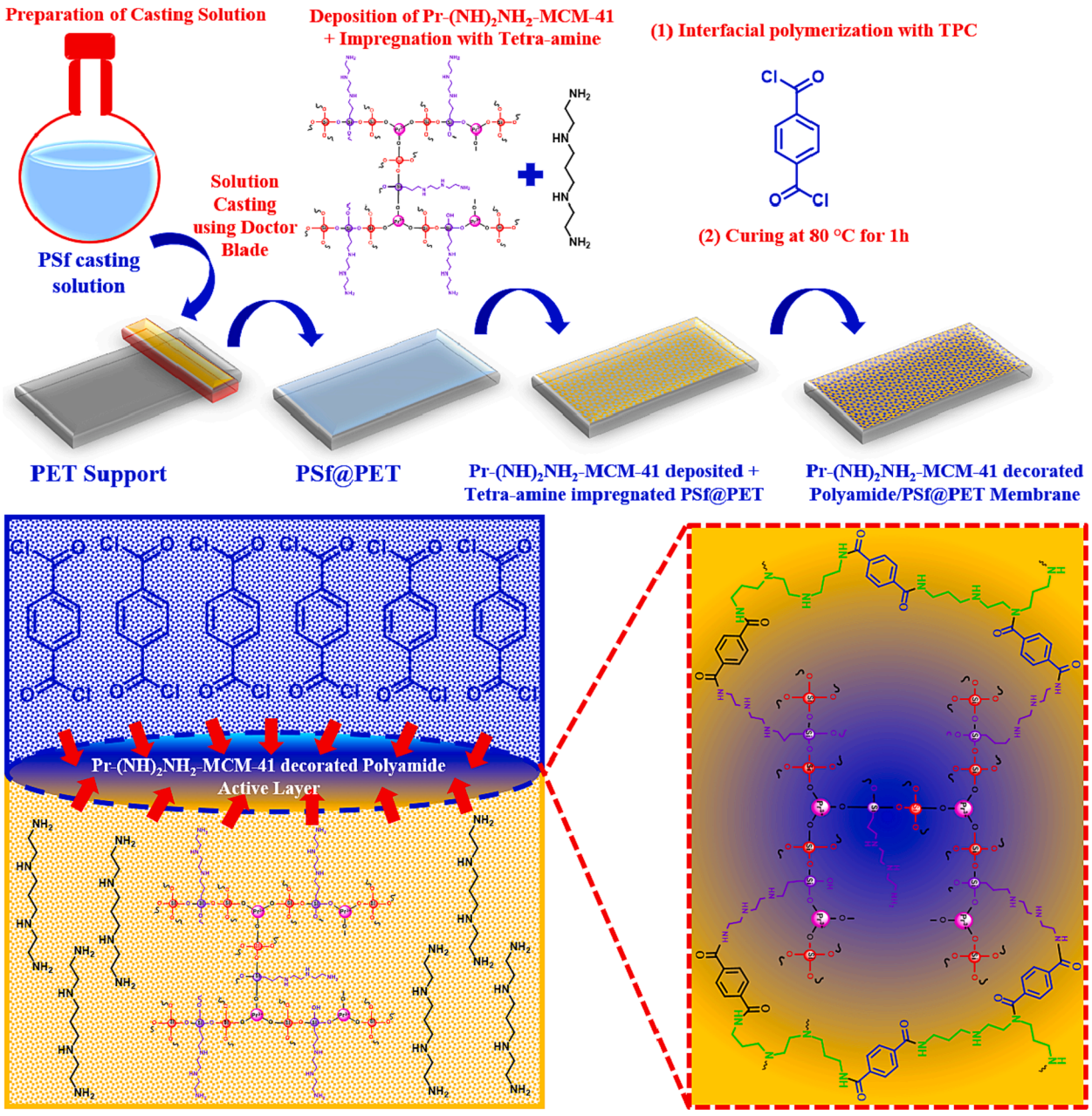

Fig. 1. Schematic illustration of steps involved in membrane fabrication through interfacial polymerization.

framework (Fig. 2). The Pr-$(NH)_2NH_2$-MCM-41 material has unique features such as large particle size and pore size which can be attributed to the presence of three methoxyethoxide groups. The zeolite framework grows from three –OH groups of trivalent PrO compared to four sides of TEOS leading to a relatively bigger pore size. Moreover, the amine groups present due to TMSPTA can act as ligands for binding with Pr transition metal resulting the formation of a complex as has been reported in literature (Kanesato et al., 1996) and on the other hand amino groups also take part in IP. A schematic representation of a possible route for the synthesis of Pr-$(NH)_2NH_2$-MCM-41 is given in Fig. 3.

Following an in-situ covalent decoration of the Pr metal ions in the structure of MCM-41 with simultaneous amino-functionalization yielding Pr-$(NH)_2NH_2$-MCM-41, various relevant characterization techniques were applied for establishing the structure of Pr-$(NH)_2NH_2$-MCM-41. To find out various functionalities in the structure of Pr-$(NH)_2NH_2$-MCM-41, FTIR was carried out as shown in Fig. 4a. The presence of amino groups can be confirmed by a broadband that spans from a region of 3600 cm^{-1} to 3200 cm^{-1} (Waheed et al., 2023a). Similarly, the aliphatic $–CH_2$ groups of Pr-$(NH)_2NH_2$-MCM-41 can also be confirmed by small peaks at 2900 cm^{-1} and 2800 cm^{-1}. The presence of a deep band at 1400 cm^{-1} can be attributed to the O-Si-O bonds of MCM-41(Waheed et al., 2023b). Similarly, a weak band at around 500 cm^{-1} can be attributed to the Pr-O bond of the Pr-$(NH)_2NH_2$-MCM-41 (Kumar Trivedi et al., 2015). After identifying the various functionalities contributing to the structure of Pr-$(NH)_2NH_2$-MCM-41, the crystal structure of Pr-$(NH)_2NH_2$-MCM-41 was studied through low-angle and wide-angle PXRD of the Pr-$(NH)_2NH_2$-MCM-41 as shown in the following Fig. 4b and 1c. The low angle XRD revealed the presence of two highly sharp peaks in a region below 1° which is a confirmation of the highly ordered structure of Pr-$(NH)_2NH_2$-MCM-41 indicating that the original structure of MCM-41 is intact even after incorporation of transition metal Pr. The wide-angle XRD also showed a typical XRD pattern of mesoporous silica MCM-41 with a hump located at 28° (Trisunaryanti et al., 2020). Hence, the low-angle and wide-angle PXRD

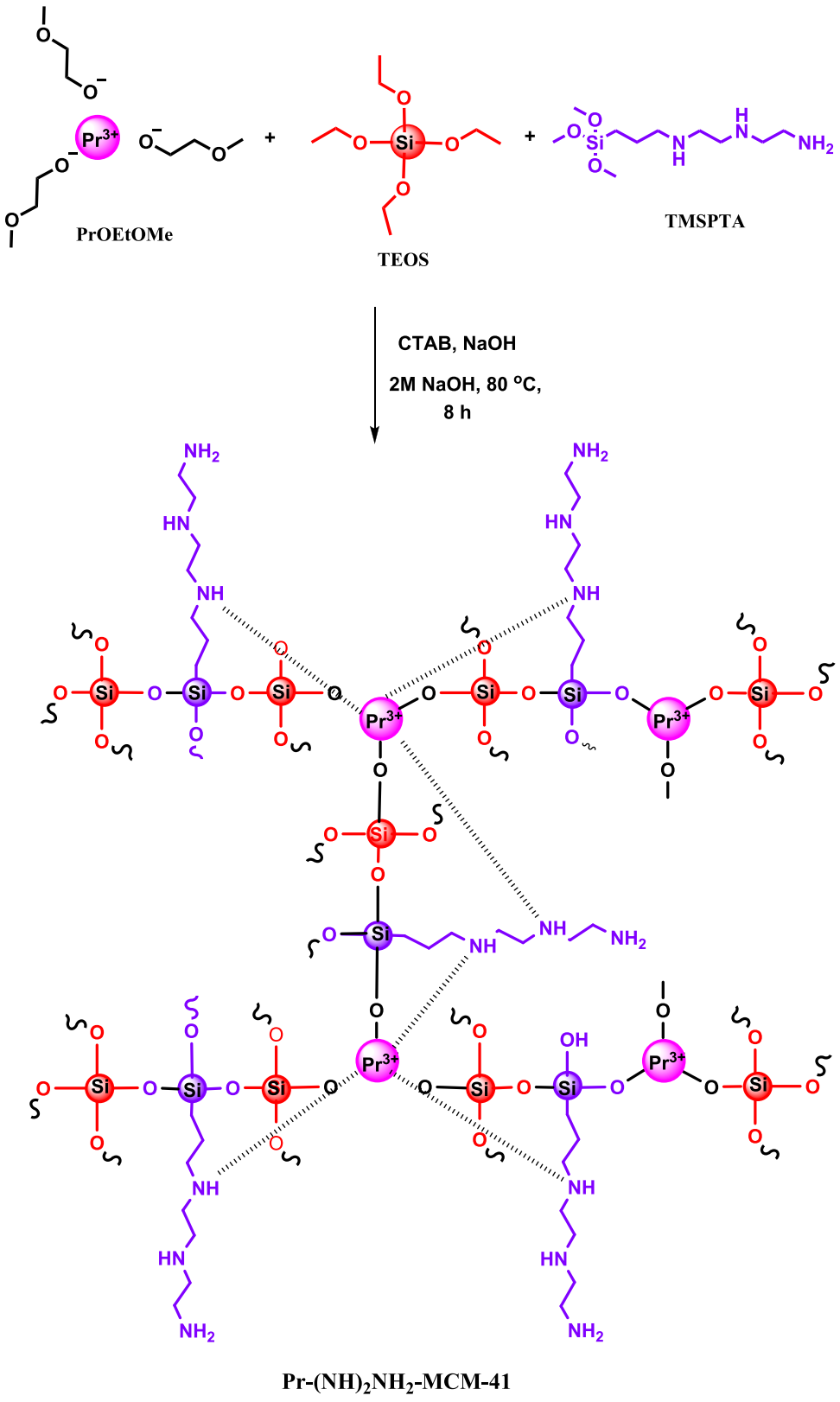

Fig. 2. Schematic representation of synthesis route of Pr-$(NH)_2NH_2$-MCM-41.

patterns confirmed the intactness of the mesoporous structure of the newly synthesized Pr-$(NH)_2NH_2$-MCM-41.

To get further evidence of the mesoporous nature of the newly synthesized Pr-$(NH)_2NH_2$-MCM-41, N_2 adsorption–desorption experiments were carried out as shown in Fig. 5a and 5b. The mesoporous nature of Pr-$(NH)_2NH_2$-MCM-41 was confirmed from the type IV isotherm of N_2 adsorption–desorption data(Ambroz et al., 2018). This type of isotherm with hysteresis loop generally develops for mesoporous materials with pores size greater than critical pore size. The capillary condensation happens at a considerably higher relative pressure P/P_o which hints at

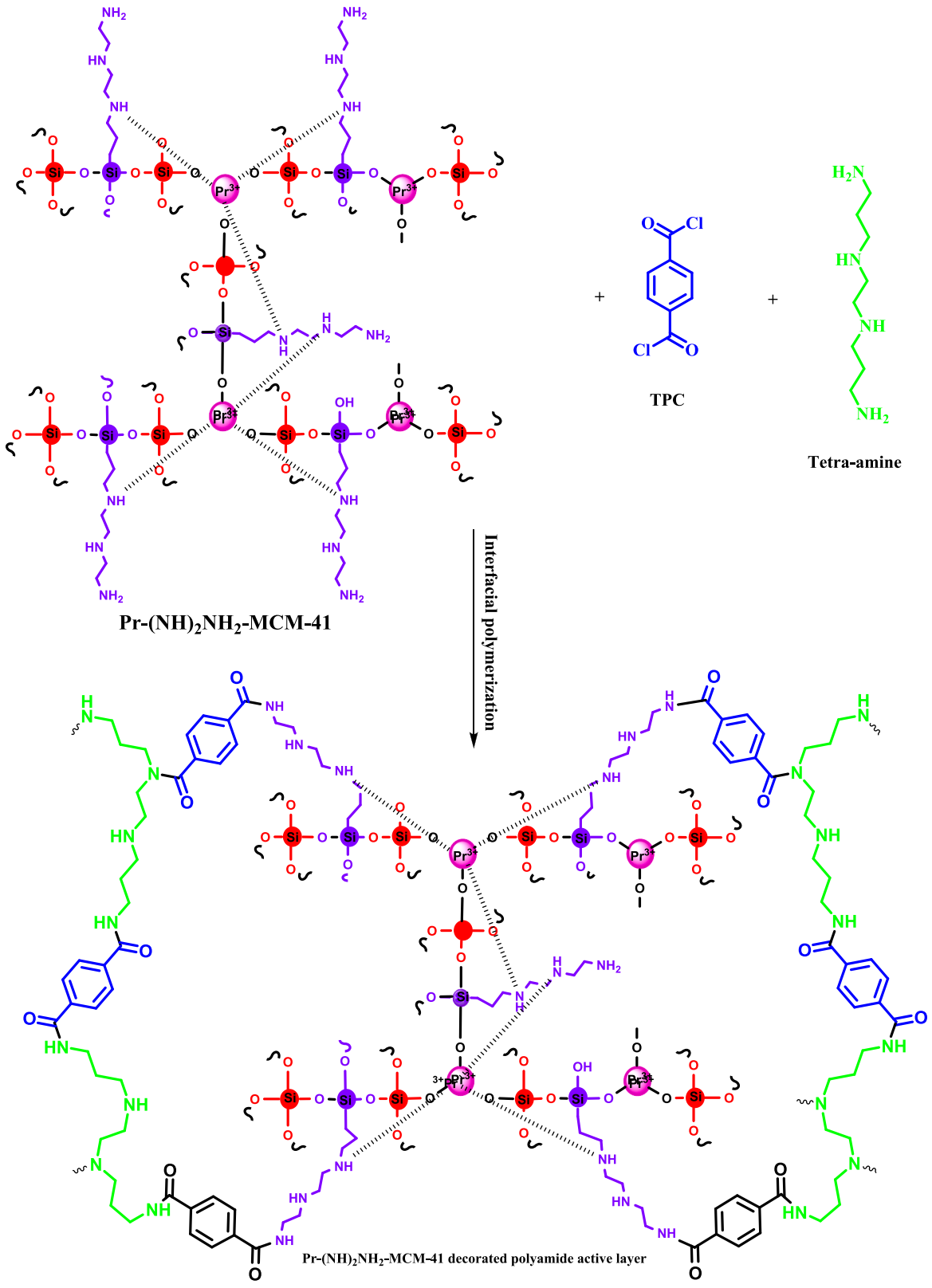

Fig. 3. Possible reaction between Pr-$(NH)_2NH_2$-MCM-41, TPC and tetra-amine during interfacial polymerization.

larger pore diameters as higher pressure of gases are required to saturate the pores completely (Fig. 5a). The pore diameter was estimated to be in the range of 3.0 nm to 4.0 nm as the half pore width was measured to be in the range of 1.5 nm to 2.0 nm (Fig. 5b). Similar results have also been found in literature(Hiratsuka et al., 2017). The surface area of the Pr-$(NH)_2NH_2$-MCM-41 was found to be 216 $m^2\ g^{-1}$. The TEM images of Pr-$(NH)_2NH_2$-MCM-41 revealed highly ordered mesoporous spherical particles (Fig. 5c). The scale shown in Fig. 5c suggested an approximate particle size ranging from 500 nm to 600 nm. The high-resolution TEM of Pr-$(NH)_2NH_2$-MCM-41 revealed uniform pore channels distributed

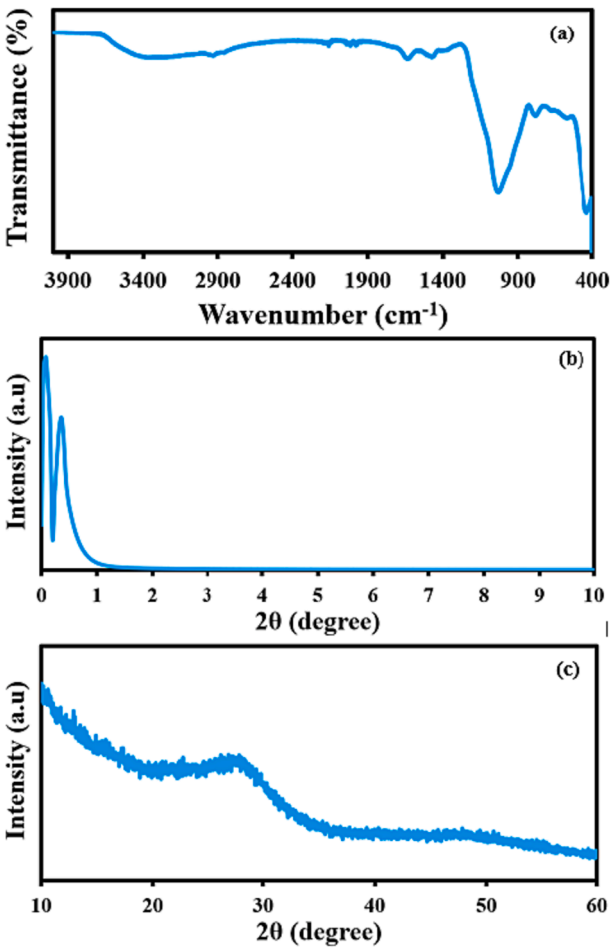

Fig. 4. (a) FTIR spectrum, (b) low angle PXRD, and (c) wide angle PXRD of Pr-$(NH)_2NH_2$-MCM-41.

throughout the structure of the Pr-$(NH)_2NH_2$-MCM-41 (Fig. 5d). The pore channels have diameters with a width of roughly 1 nm to 2 nm which agrees with the BET data. Hence, the structural and morphological features of the Pr-$(NH)_2NH_2$-MCM-41 make them a perfect choice for application in the separation of desired solutes and filtration of micropollutants.

To ascertain the chemical composition of the Pr-$(NH)_2NH_2$-MCM-41, EDX and mapping analysis of Pr-$(NH)_2NH_2$-MCM-41 were carried out as shown in Fig. 6. When an appropriate area of Pr-$(NH)_2NH_2$-MCM-41 (Fig. 6a) was analyzed through EDX, it revealed the presence of all the constituent elements in Pr-$(NH)_2NH_2$-MCM-41. The elements include Carbon (C), Oxygen (O), Nitrogen (N), and more importantly Silicon (Si) and Praseodymium (Pr). The presence of C and O can be attributed to Tetraethyl orthosilicate (TEOS), and Praseodymium methoxyethoxide (PrOMeEtO) while N is due to N1-(3-Trimethoxy silylpropyl) diethylenetriamine (TMSPTA). The lower content of N compared to other elements is in perfect agreement with the molecular structure of the reactants where TMSPTA is a sole contributor of N to the structure of Pr-$(NH)_2NH_2$-MCM-41. Similarly, Si is due to silane groups of TEOS and TMSPTA while Pr is due to PrOMeEtO. These results confirmed the contribution of all the constituent elements towards the structure of Pr-$(NH)_2NH_2$-MCM-41 (Fig. 6b). The mapping analysis confirmed the uniform distribution of all the detected elements in the structure of Pr-$(NH)_2NH_2$-MCM-41 (Fig. 6c to 6 g). Another observation is the density of the elements in the Pr-$(NH)_2NH_2$-MCM-41 which is directly related to the concentration of elements in Pr-$(NH)_2NH_2$-MCM-41.

The Pr-$(NH)_2NH_2$-MCM-41 was decorated through covalent cross-linking of Pr-$(NH)_2NH_2$-MCM-41 in the active layer of the membranes. Both primary and secondary amino groups of Pr-$(NH)_2NH_2$-MCM-41 are responsible for covalently bonding the Pr-$(NH)_2NH_2$-MCM-41 in the polyamide active layer of the membranes. The amide bonds are formed between acyl chloride groups of TPC and amino groups of Pr-$(NH)_2NH_2$-MCM-41 and tetra-amine (Jillani et al., 2022). Hence, due to the chemical bonding between the amino groups and acyl chloride groups, Pr-$(NH)_2NH_2$-MCM-41 is covalently bonded in the membrane active layer. This stable incorporation of Pr-$(NH)_2NH_2$-MCM-41 in the active layer of the membranes is a highly desirable feature for membranes because Pr-$(NH)_2NH_2$-MCM-41 will remain stable during filtration experiments. The possible reaction between Pr-$(NH)_2NH_2$-MCM-41, TPC, and tetra-amine along with the structure of the polyamide active layer is

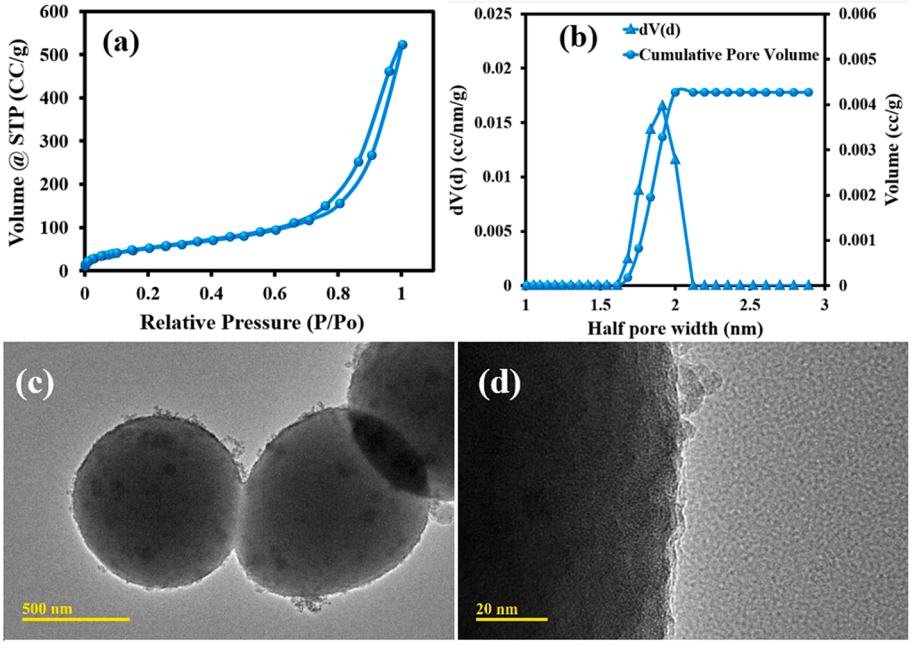

Fig. 5. (a) The BET isotherm, (b) pore width, (c and d) TEM images of Pr-$(NH)_2NH_2$-MCM-41.

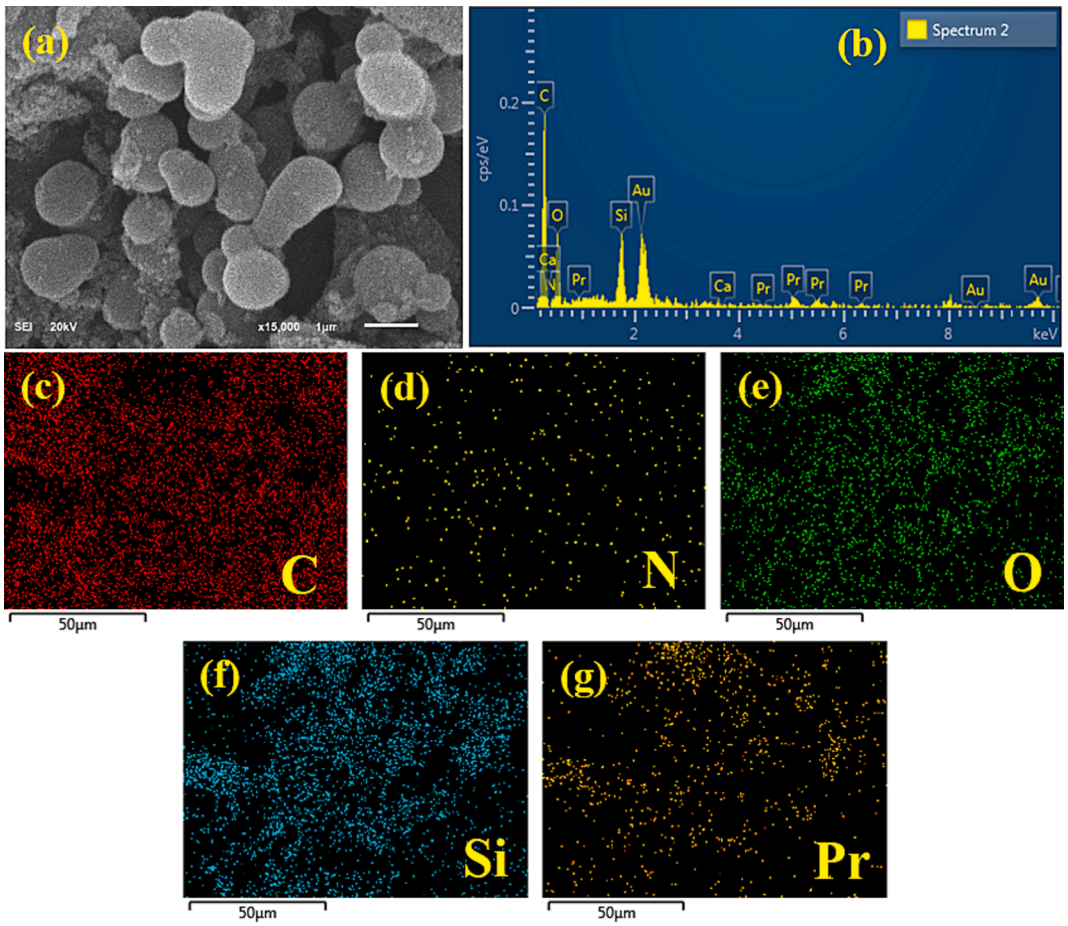

Fig. 6. (a) The selected area, (b) EDX analysis, and (c to g) mapping analysis of Pr-$(NH)_2NH_2$-MCM-41 [0.05%].

given in Fig. 3.

Free-standing active layers of the three different concentrations of Pr-$(NH)_2NH_2$-MCM-41 were synthesized for the sake of establishing and characterizing the structures of the Pr-$(NH)_2NH_2$-MCM-41 decorated membranes. FTIR analysis of free-standing active layers revealed the presence of several functional groups confirming the structure and functionalities of Pr-$(NH)_2NH_2$-MCM-41 membranes (Fig. 7a and 7b). As all the active layers are polyamides in nature, the presence of an amide bond (–CONH) was realized by the presence of a broad band in a region of 3600 cm^{-1} to 3200 cm^{-1} which is a characteristic peak due to –N–H stretching of an amide linkage. The amide bonds are generated due to the reaction of acid chloride (-COCl) of TPC with amine ($–NH_2$) groups of Pr-$(NH)_2NH_2$-MCM-41 and tetra-amine. The other important peaks include aromatic –C–H bond stretching at around 3000 cm^{-1} due to

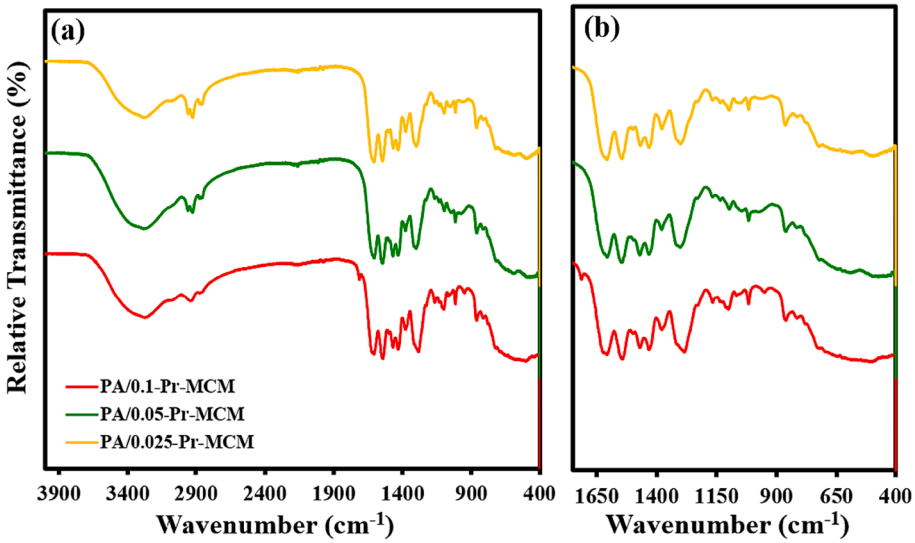

Fig. 7. (a) ATR-FTIR spectra and (b) fingerprint region of Pr-$(NH)_2NH_2$-MCM-41 decorated active layers of the membranes.

benzene rings of TPC, -C–H bond stretching at 2900 cm^{-1} and 2800 cm^{-1} due to aliphatic linear chains of tetra-amine and Pr-$(NH)_2NH_2$-MCM-41. Another confirmatory peak of amide linkage is the carbonyl (>C = O) peak which is located at 1650 cm^{-1}. Furthermore, a peak located at around 1300 cm^{-1} to 1200 cm^{-1} is due to O-Si-O of Pr-$(NH)_2NH_2$-MCM-41. All these findings and observations verified an effective contribution of all the reacting monomers leading to the co-valent decoration of Pr-$(NH)_2NH_2$-MCM-41 in the active layers of the membranes.

Following Fig. 8 shows the ATR-FTIR spectra of all the TFC membranes compared to PSU/PET support. Appropriate and completely dried pieces of the support and fabricated membranes were scanned in ATR mode for recording the FTIR spectra. All the membranes with different concentrations of Pr-$(NH)_2NH_2$-MCM-41 showed the presence of all the peaks identified in the case of free-standing active layers as shown in Fig. 7. However, in the case of PSU/PET support, the region from 3600 cm^{-1} to 3200 cm^{-1} was found devoid of the broad amide peak as the PSU/PET support lacks the polyamide active layer (Fig. 8a and 8b).

After establishing the chemical structure of Pr-$(NH)_2NH_2$-MCM-41 decorated membranes and PSU/PET support, various surface features of the support and membranes were also revealed by different characterization techniques. AFM of the support and Pr-$(NH)_2NH_2$-MCM-41 decorated membranes are given in Fig. 9. AFM of the PSU/PET support (Fig. 9a and 9b) revealed a comparatively smoother surface compared to Pr-$(NH)_2NH_2$-MCM-41 decorated membranes. The smooth surface of PSU/PET support is attributed to the uniform and smooth deposition of a polysulfone dope solution using a doctor's blade on unwoven PET. After the IP reaction, the development of Pr-$(NH)_2NH_2$-MCM-41 decorated polyamide active layer resulted in the formation of a characteristic ridge and valley structure on PSU/PET support. A careful analysis of both 2D and 3D AFM images led to the conclusion that the overall surface roughness of the Pr-$(NH)_2NH_2$-MCM-41 decorated membranes decreased with increasing concentration of Pr-$(NH)_2NH_2$-MCM-41. The highest surface average roughness (R_a) and mean square roughness (R_q) was found for PA/0.025-Pr-MCM@PSU/PET with R_a and R_q values of 28.4 nm and 33.2 nm respectively (Fig. 9c and 9d). As the Pr-$(NH)_2NH_2$-MCM-41 concentration was raised to 0.05 %, the R_a and R_q values decreased to 20.6 nm and 25.3 nm respectively (Fig. 9e and 9f). Finally, with a Pr-$(NH)_2NH_2$-MCM-41 concentration of 0.10 % in case of PA/0.10-Pr-MCM@PSU/PET membrane the R_a and R_q values were decreased further to 16.5 nm and 19.4 nm (Fig. 9g and 9 h). This trend can be attributed to the effective contribution of Pr-$(NH)_2NH_2$-MCM-41 in the crosslinking event of IP. The contribution of Pr-$(NH)_2NH_2$-MCM-41 in crosslinking leads to filling of the valleys between the ridges of the polyamide beads which can be clearly seen in the 3D images of membranes as shown in Fig. 9d, 9f and 9 h. The presence of amino groups in the structure of Pr-$(NH)_2NH_2$-MCM-41 made the covalent crosslinking of Pr-$(NH)_2NH_2$-MCM-41 in the active layer of the membranes.

Another highly useful characteristic feature of membranes is the surface hydrophilicity of the membranes. The water contact angle (WCA) measurement showed a value of 90° which is consistent with several hand cast polyamide membranes reported in literature(Pang and Zhang, 2017). These higher values of handmade polyamide membranes compared to commercial membranes are due to the rougher surface. Due to the increased surface roughness of polyamide membranes, larger WCA contact angles are obtained than expected from the chemistry of the membrane which is due to the entrapment of air bubbles between the solid surface rugosities and water droplets(Ni and Ge, 2018). It was observed that the WCA increased with increasing concentration of Pr-$(NH)_2NH_2$-MCM-41 in the active layer of the membrane as PA/0.025-Pr-MCM@PSU/PET and PA/0.050-Pr-MCM@PSU/PET have WCAs of 90° and 95°, respectively (Fig. 10). This increase in WCA shows that Pr-$(NH)_2NH_2$-MCM-41 is relatively less hydrophilic which might be due to the presence of silane groups in the structure of Pr-$(NH)_2NH_2$-MCM-41. However, in the case of PA/0.100-Pr-MCM@PSU/PET membrane, WCA was decreased to 85° which might be due to smoother surface (R_a = 16.5 nm) of PA/0.100-Pr-MCM@PSU/PET membrane compared to PA/0.025-Pr-MCM@PSU/PET (R_a = 28.4 nm) and PA/0.050-Pr-MCM@PSU/PET (R_a = 20.6 nm).

Like surface roughness and hydrophilicity of the membranes, surface morphology of the membranes is also a highly important feature of membranes. Fig. 11 shows SEM micrographs of all the fabricated membranes including PSU/PET support. Fig. 11a to 11c shows the micrographs of PSU/PET support at different magnifications. The PSU/PET support appears highly porous and shows a uniform structure. This highly porous structure of PSU/PET support is due to the phase inversion process as the DMAc leaves the PSU and water replaces the DMAc leading to the development of pores in PSU/PET support. In contrast to PSU/PET support, the surface of the membranes appeared highly beaded having a typical ridge and valley configuration. This ridge and valley morphology of the Pr-$(NH)_2NH_2$-MCM-41 membrane is attributed to the

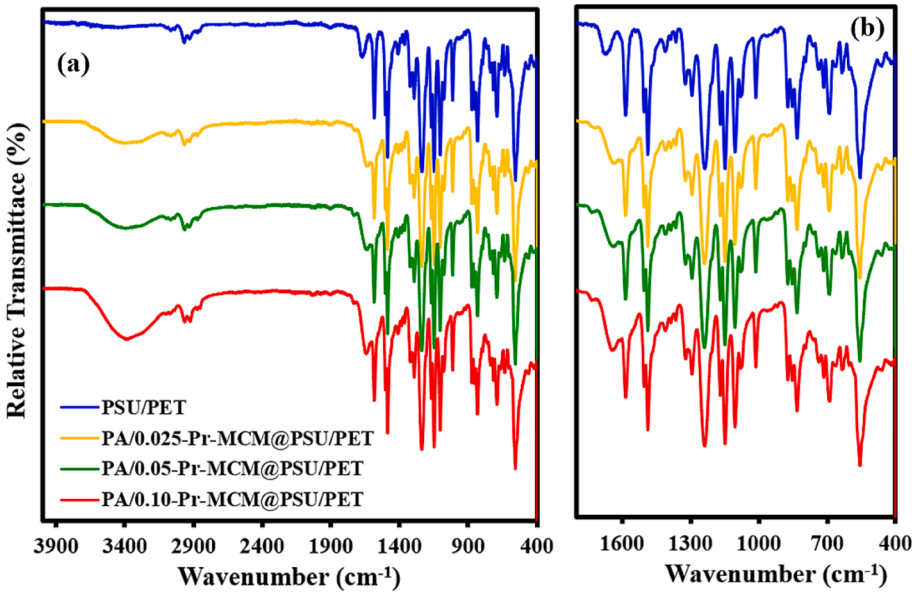

Fig. 8. (a) ATR-FTIR spectra and (b) fingerprint region of Pr-$(NH)_2NH_2$-MCM-41 decorated membranes and PSU/PET support.

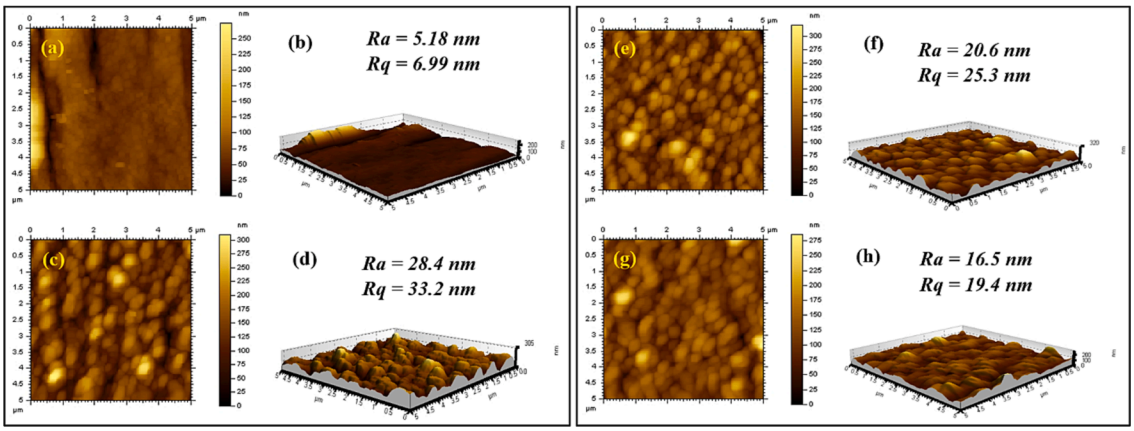

Fig. 9. AFM images of (a and b) PSU/PET support, (c and d) PA/0.025-Pr-MCM@PSU/PET, (e and f) PA/0.050-Pr-MCM@PSU/PET and (g and h) PA/0.100-Pr-MCM@PSU/PET decorated membranes and PSU/PET support.

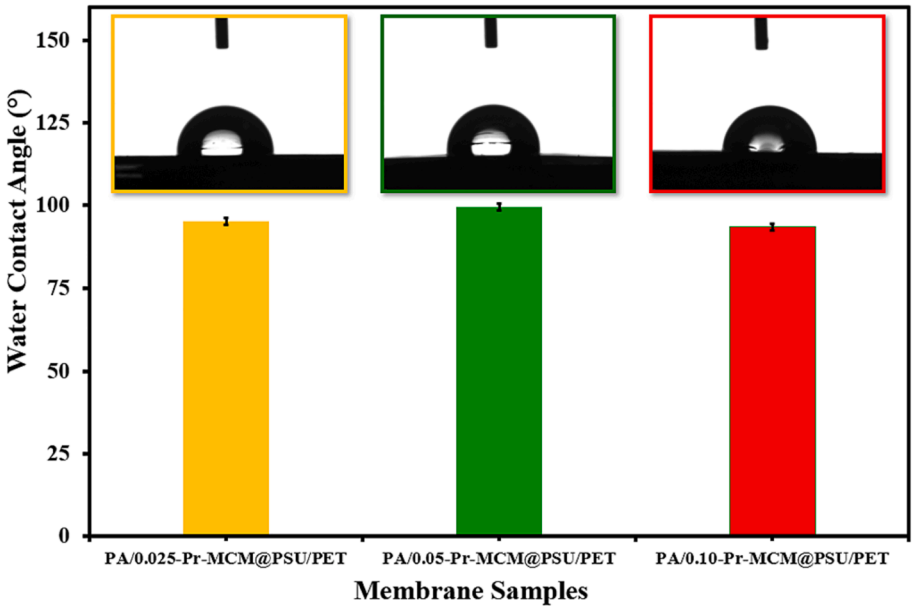

Fig. 10. Water contact angles of PA/0.025-Pr-MCM@PSU/PET, PA/0.050-Pr-MCM@PSU/PET and PA/0.100-Pr-MCM@PSU/PET.

successful IP reaction between Pr-$(NH)_2NH_2$-MCM-41 containing aqueous amine solution and non-aqueous hexane solution of TPC. A careful analysis of micrographs of Pr-$(NH)_2NH_2$-MCM-41 decorated membranes showed that with increasing concentration of Pr-$(NH)_2NH_2$-MCM-41, the valleys get filled with the polymeric mass, and the membrane surface becomes relatively smooth as confirmed by AFM analysis of the membrane. Fig. 11f shows that PA/0.025-Pr-MCM@PSU/PET membrane has more vivid and clear valleys while in the case of PA/0.050-Pr-MCM@PSU/PET membrane, the ridges become slightly smoother (Fig. 11i). Similarly, a smoother morphology is observed in case of PA/0.100-Pr-MCM@PSU/PET (Fig. 11m). The SEM micrographs of the Pr-$(NH)_2NH_2$-MCM-41 decorated membranes revealed the fact that Pr-$(NH)_2NH_2$-MCM-41 was completely impregnated throughout the entire area of the membrane and no agglomeration of Pr-$(NH)_2NH_2$-MCM-41 was seen (Fig. 11d to 11 m). This is due to the introduction of organic components such as TMSPTA which made Pr-$(NH)_2NH_2$-MCM-41 familiar with the polymeric polyamide active layer. Given the unique features of Pr-$(NH)_2NH_2$-MCM-41 such as porosity, particle size, and surface area, the uniform decoration of Pr-$(NH)_2NH_2$-MCM-41 in the polyamide active layer provides the membranes with unique separation potential. Moreover, the ridge and valley confirmation of the membranes provides routes for the transport of water while rejecting the solutes.

To further confirm the incorporation of Pr-$(NH)_2NH_2$-MCM-41 in the polyamide active layer of the TFC membranes, EDX analysis of the PUS/PET support and all the fabricated membranes was carried out as shown in the following Fig. 12. As expected from the molecular structure of PSU/PET, EDX analysis of a selected area of PSU/PET support (Fig. 12a) confirmed the presence of carbon (C), sulfur (S) and oxygen (O) (Fig. 12b). However, EDX analysis of selected areas of Pr-$(NH)_2NH_2$-MCM-41 decorated membranes (Fig. 12c, 12e and 12 g) disclosed the presence of two additional elements nitrogen (N) and Praseodymium (Pr) which are due to the polyamide (–CONH) nitrogen atoms and Pr present in Pr-$(NH)_2NH_2$-MCM-41 (Fig. 12d, 12f and 12 h). These observations confirmed the successful decoration of Pr-$(NH)_2NH_2$-MCM-41 in the polyamide active layer of the membranes.

After confirming the presence of various essential elements in the active layer of the membranes, the distribution of all the elements in the active layer showed that all the identified elements were equally distributed throughout the entire area of the membranes (Fig. 13). The relative amount of all the elements in the membranes are reflected in the intensity of the colored dots in the images of the respected element. C

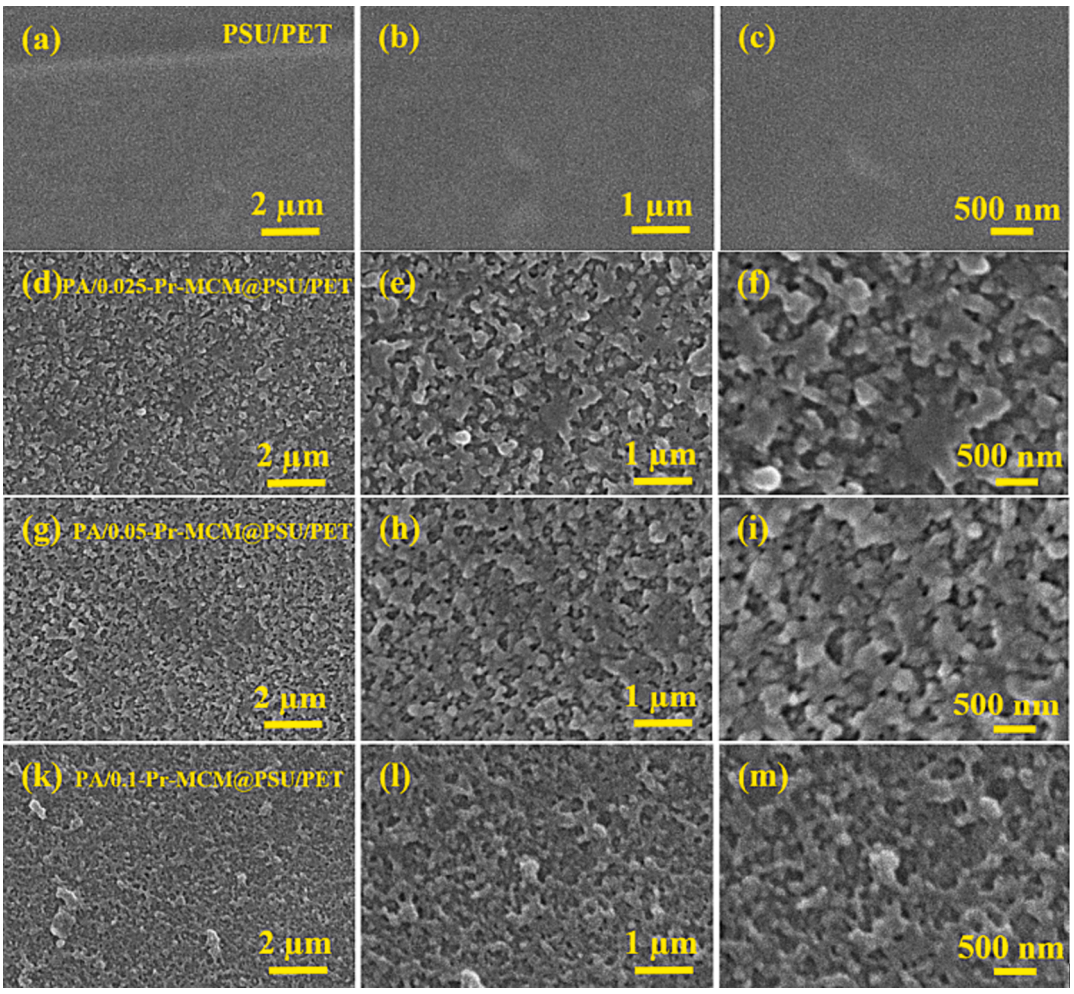

Fig. 11. SEM micrographs of (a to c) PSU/PET support, (d to f) PA/0.025-Pr MCM@PSU/PET, (g to i) PA/0.050-Pr-MCM@PSU/PET and (k to m) PA/0.100-Pr-MCM@PSU/PET.

(Fig. 13a) and S (Fig. 13e) are the most abundant elements followed by O (Fig. 13c) and Si (Fig. 13d) while N (Fig. 13b) and Pr (Fig. 13f) are the least abundant elements which agree with the molecular composition of membranes. These findings suggested that the Pr-$(NH)_2NH_2$-MCM-41 were successfully decorated in the polyamide active layer of the membranes where it has become an integral part of the membranes.

Following thorough characterization and establishing the structure of the membranes, the filtration performance of the Pr-$(NH)_2NH_2$-MCM-41 decorated membranes was evaluated. All three membranes were installed in parallel on a crossflow filtration system and DI water was used as feed for compacting the membranes for 1 h at 20 bar. Following compaction, the membranes were tested for variation in the flux with increasing transmembrane pressure from 5 bar to 25 bar (Fig. 14). It was observed that the permeate flux increased linearly with increasing transmembrane pressure with flux reaching 56 L $m^{-2}h^{-1}$ (LMH) at 25 bar for PA/0.050-Pr-MCM@PSU/PET membrane. Among the three tested membranes, the permeate flux showed variations to a certain extent, and following trend of increasing permeate flux was found PA/0.050-Pr-MCM@PSU/PET < PA/0.025-Pr-MCM@PSU/PET < PA/0.100-Pr-MCM@PSU/PET membrane. The permeate flux was found to be 33 LMH, 42 LMH, and 56 LMH at 25 bar for PA/0.050-Pr-MCM@PSU/PET, PA/0.025-Pr-MCM@PSU/PET and PA/0.100-Pr-MCM@PSU/PET respectively. This variation in permeate flux reflected that the amount of Pr-$(NH)_2NH_2$-MCM-41 decorated in the membrane active layer has affected the structure of the polyamide active layer. These variations in membrane structure have already been detected during membrane characterization such as SEM, AFM, and WCA. The 0.025 wt% led to an active layer with big-sized polyamide globules (Fig. 11f) while 0.100 wt % of Pr-$(NH)_2NH_2$-MCM-41 resulted in highly fine fibrous and porous active layers (Fig. 11m) of the membranes. These features could be possibly responsible for higher flux in the case of PA/0.025-Pr-MCM@PSU/PET and PA/0.100-Pr-MCM@PSU/PET membranes. However, in the case of 0.05 % wt% loading of Pr-$(NH)_2NH_2$-MCM-41 has generated a highly uniform and dense polyamide active layer which is responsible for lower permeate flux in the case of PA/0.050-Pr-MCM@PSU/PET membrane.

Similarly, the rejection performance of membranes was also tested by using both divalent (Mg^{2+}, Ca^{2+}, and SO_4^{2-}) and monovalent ions (Na^+ and Cl^-). By comparing the rejection performance of the fabricated membranes, it was found that the use of higher concentrations of Pr-$(NH)_2NH_2$-MCM-41 in the active layers of the fabricated membranes was not a suitable option for gaining performance improvements. The PA/0.100-Pr-MCM@PSU/PET membrane showed the lowest rejection among all the three fabricated membranes which can be understood by considering the structural features of the PA/0.100-Pr-MCM@PSU/PET membrane. Both SEM micrographs and AFM analysis of the PA/0.100-Pr-MCM@PSU/PET membrane revealed an active layer having reduced ridge and valley configuration and the lowest surface roughness among all the membranes. Hence, the PA/0.100-Pr-MCM@PSU/PET membrane offered the lowest mass transfer resistance to both the salts and permeating water through the membrane. In the case of PA/0.100-Pr-MCM@PSU/PET membrane, the rejections of $CaCl_2$, $MgCl_2$, Na_2SO_4,

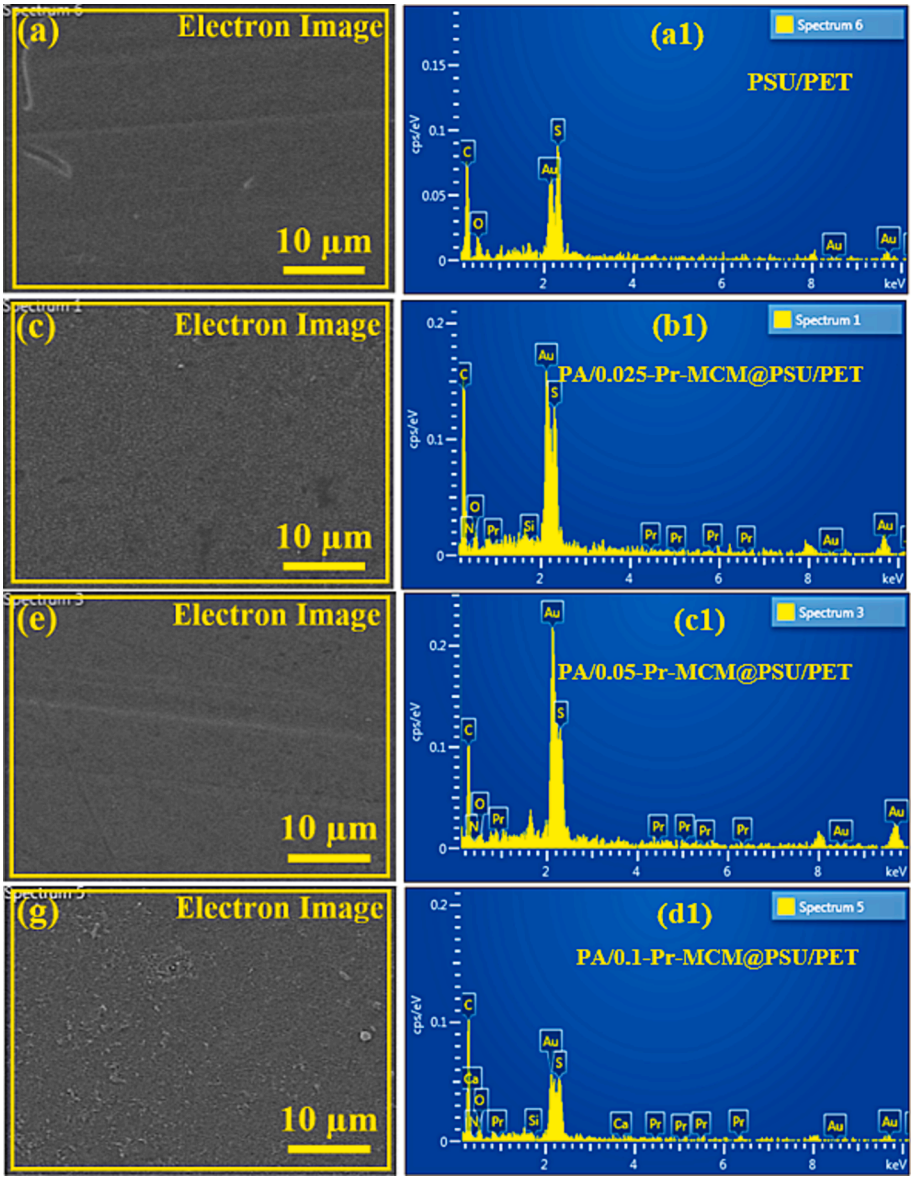

Fig. 12. Selected areas for EDX of (a) PSU/PET support, (c) PA/0.025-Pr-MCM@PSU/PET, (e) PA/0.050-Pr-MCM@PSU/PET and (g) PA/0.100-Pr-MCM@PSU/PET and EDX analysis of (b) PSU/PET support, (d) PA/0.025-Pr-MCM@PSU/PET, (f) PA/0.050-Pr-MCM@PSU/PET and (h) PA/0.100-Pr-MCM@PSU/PET.

$MgSO_4$, and NaCl were found to be 72 %, 62 %, 58 %, 55 %, and 48 % respectively. The structure of Pr-$(NH)_2NH_2$-MCM-41 can also contribute to the decrease in the rejection of salts. Hence, higher concentrations of Pr-$(NH)_2NH_2$-MCM-41 are not ideal for enhancing the performance of the membranes which might be due to the larger particle size and pore size of Pr-$(NH)_2NH_2$-MCM-41. Therefore, the lower concentrations of Pr-$(NH)_2NH_2$-MCM-41 were found to be highly suitable for enhancing the flux of the membranes while maintaining relatively higher salt rejections. The rejection of salts by PA/0.05-Pr-MCM@PSU/PET membrane was found to be the highest among all the fabricated membranes which were found to be 98 %, 96 %, 95 %, 87 %, and 82 % for $CaCl_2$, $MgCl_2$, $MgSO_4$, Na_2SO_4 and NaCl, respectively. Similarly, the PA/0.025-Pr-MCM@PSU/PET membrane also showed a similar rejection of salts to that of the PA/0.05-Pr-MCM@PSU/PET membrane. Hence, the lower doses of Pr-$(NH)_2NH_2$-MCM-41 were found to be suitable for fabricating a desalination membrane with considerably acceptable salt rejection without lowering permeate flux to a larger extent. Salts are rejected by various mechanisms which include size exclusion and charge exclusion. As it has been observed in the current pattern of salt rejection, the divalent ions such as Ca^{2+}, Mg^{2+}, and SO_4^{2-} have higher rejection than monovalent ions such as Na^{+}. The highest salt rejection was recorded for $CaCl_2$ where Ca^{2+} is the largest ion studied in the current work. Another interesting example is the rejection of $MgSO_4$ and Na_2SO_4 where $MgSO_4$ showed a rejection of 95 %, whereas Na_2SO_4 was rejected up to 87 %. The higher rejection of $MgSO_4$ can be attributed to the fact that both Mg^{2+} and SO_4^{2-} are divalent ions having larger ionic radii causing higher salt rejection. Hence, the salient features of Pr-$(NH)_2NH_2$-MCM-41 such as porosity, pore size, particle size, surface area, hydrophilicity, and compatibility with the polyamide active layer contribute to the enhanced performance of the desalination membranes. To get a highly optimized performance of an additive such as zeolites decorated in the active layer of the membranes, more attention should be dedicated to optimizing the concentration of the additive. Moreover, another important aspect of the development of high-performance membranes using inorganic additives is to introduce an organic component to enhance its homogeneity to the polymeric active layer. Therefore, the current work was focused on introducing organic functionalization to Pr-$(NH)_2NH_2$-MCM-41 and optimizing its concentration.

Fig. 15 shows the rejection performance of the membranes by using different well-known pharmaceuticals as micropollutants in the feed.

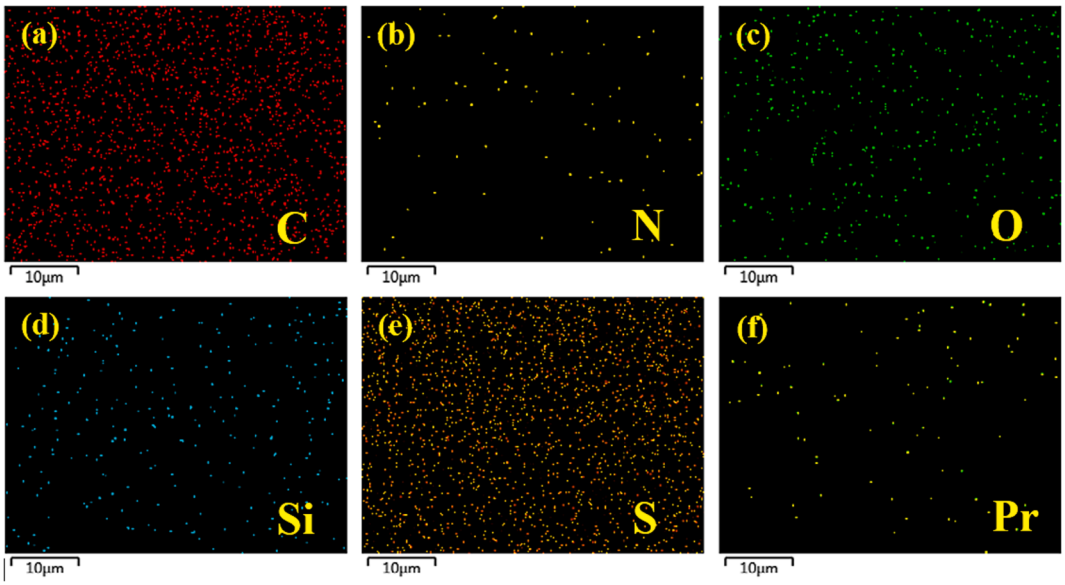

Fig. 13. Mapping analysis of PA/0.050-Pr-MCM@PSU/PET membranes as a representative membrane.

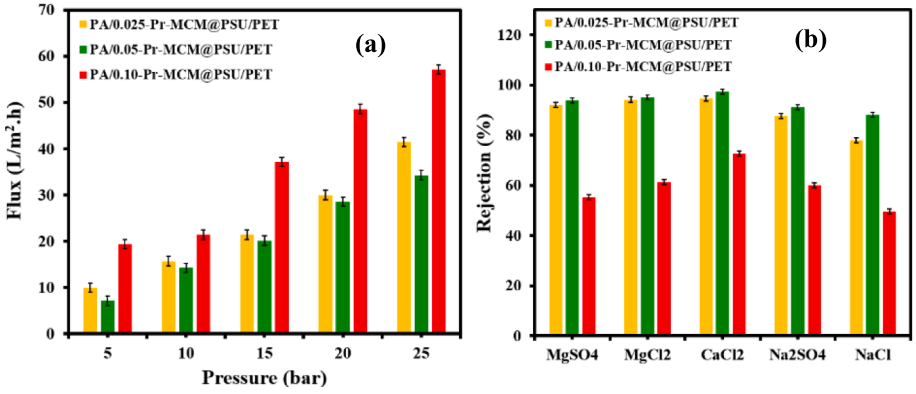

Fig. 14. (a) Effect of pressure on permeate flux and (b) salt rejection by PA/0.025-Pr-MCM@PSU/PET, PA/0.050-Pr-MCM@PSU/PET, and PA/0.100-Pr-MCM@PSU/PET.

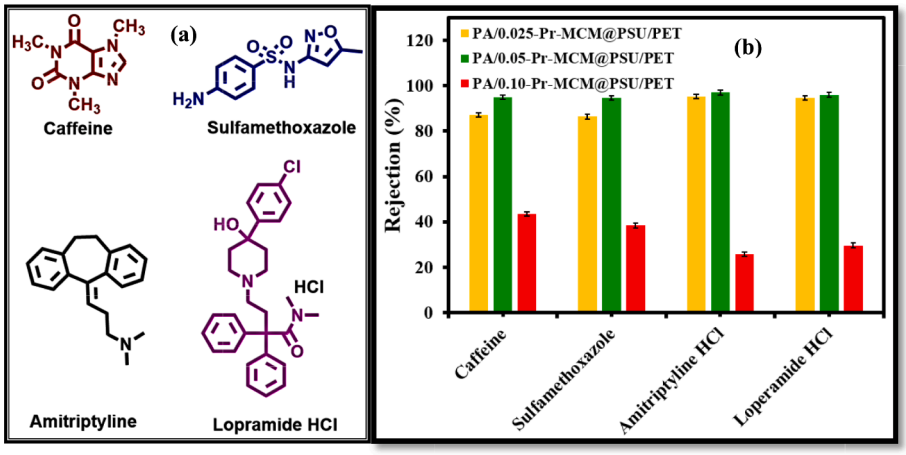

Fig. 15. (a) Structures of pharmaceuticals and (b) rejection of pharmaceuticals by PA/0.025-Pr-MCM@PSU/PET, PA/0.050-Pr-MCM@PSU/PET, and PA/0.100-Pr-MCM@PSU/PET.

The micropollutants are continuously increasing in water bodies and hence require treatment before disposal as well as reuse of the contaminated water. All the pharmaceutical drugs (Fig. 15a) were found to be highly rejected > 96 % by PA/0.5-Pr-MCM-41@PSU/PET membrane followed by PA/0.025-Pr-MCM-41@PSU/PET membrane. The higher rejection of micropollutants by the PA/0.5-Pr-MCM-41@PSU/

PET membrane can be attributed that the molecular weights of the drugs studied in this work lie above the molecular weight cutoff (MWCO) of the membrane. Hence due to the larger size of the molecules, the drugs are rejected > 96 %.

Since, the Pr-$(NH)_2NH_2$-MCM-41 has an ideal chemistry required for covalent bonding of Pr-$(NH)_2NH_2$-MCM-41 in the active layer of the membrane. Due to the formation of a stable covalent bond between Pr-$(NH)_2NH_2$-MCM-41 and TMC, the Pr-$(NH)_2NH_2$-MCM-41 becomes an integral part of the membrane active layer and hence their chances of washing out are reduced to a negligible level which in turn minimizes the potential environmental side effects of using rare earth elements.

4. Conclusion

An in-situ approach was used for synthesis of modified version of MCM-41 by covalently decorating PrO in the framework of MCM-41 with simultaneous amino functionalization leading to Pr-$(NH)_2NH_2$-MCM-41. Given the presence of several amino groups in the structure of Pr-$(NH)_2NH_2$-MCM-41, the interfacial polymerization successfully led to the fabrication of nanofiltration membrane with tetra-amine as additional aqueous amine. The HR-TEM revealed the existence of particles of Pr-$(NH)_2NH_2$-MCM-41 in the form of pairs with geometry like MCM-41. The low angle XRD revealed the presence of two highly sharp peaks in a region below 1° which is a confirmation for the highly ordered structure of Pr-$(NH)_2NH_2$-MCM-41 indicating that the original structure of MCM-41 is intact even after incorporation of transition metal Pr. The covalent decoration of Pr-$(NH)_2NH_2$-MCM-41 in the membrane active layer yielded membranes with different structural and functional features. The lower concentrations (0.025 %, 0.05 %) of Pr-$(NH)_2NH_2$-MCM-41 were found to be advantageous compared to higher concentrations (0.10 %) in terms of performance of the membranes. This observation is evident from the higher salt rejection by PA/0.025-Pr-MCM@PSU/PET membrane and PA/0.05-Pr-MCM@PSU/PET membrane. Therefore, PA/0.05-Pr-MCM@PSU/PET membrane rejected $CaCl_2$ up to 98 % and $MgCl_2$ up to 96 %. In terms of permeate flux, PA/0.05-Pr-MCM@PSU/PET membrane showed a permeate flux of 56 L m-2 h-1 (LMH) at 25 bar. All the pharmaceutical drugs were found to be highly rejected > 96 % by PA/0.05-Pr-MCM-41@PSU/PET membrane. Hence, when different membranes were compared, 0.5 % dose of Pr-$(NH)_2NH_2$-MCM-41 was found to be an optimum dose where PA/0.05-Pr-MCM@PSU/PET membrane showed better performance both in terms of selectivity and flux.

Declaration of competing interest

The authors declare that they have no known competing financial interests or personal relationships that could have appeared to influence the work reported in this paper.

Acknowledgement

Authors would like to acknowledge the support provided by the IRC for Membranes and Water Security through project # INMW2306 and INMW2311, King Fahd University of Petroleum and Minerals, Saudi Arabia.

References

Ahmad, N.A., Goh, P.S., Yogarathinam, L.T., Zulhairun, A.K., Ismail, A.F., 2020. Current advances in membrane technologies for produced water desalination. Desalination 493, 114643. https://doi.org/10.1016/J.DESAL.2020.114643.

Aldossari, M., 2023. Addressing Water security in arid and water stressed in KSA [WWW Document]. United Nations. URL https://sdgs.un.org/partnerships/addressing-water-security-arid-and-water-stressed-ksa.

Alsohaimi, I.H., Alrashidi, A.N., Hassan, H.M.A., Chen, Q., 2023. Highly efficient ultrafiltration membrane performance of PES@microcrystalline cellulose extracted from waste fruits for the removal of Br O3− from drinking water samples. Colloid Interface Sci. Commun. 54, 100718 https://doi.org/10.1016/j.colcom.2023.100718.

Ambroz, F., Macdonald, T.J., Martis, V., Parkin, I.P., Ambroz, F., Macdonald, T.J., Parkin, I.P., Martis, V., 2018. Evaluation of the BET theory for the characterization of meso and microporous MOFs. Small Methods 2, 1800173. https://doi.org/10.1002/SMTD.201800173.

Baig, U., Faizan, M., Waheed, A., 2022. A review on super-wettable porous membranes and materials based on bio-polymeric chitosan for oil-water separation. Adv. Colloid Interface Sci. 303 https://doi.org/10.1016/J.CIS.2022.102635.

Cao, X., Lu, J., Zhao, Y., Tian, R., Zhang, W., He, D., Luo, Y., 2021. Promotional Effects of Rare-Earth Praseodymium (Pr) Modification over MCM-41 for Methyl Mercaptan Catalytic Decomposition. Process. 2021, Vol. 9, Page 400 9, 400. https://doi.org/10.3390/PR9020400.

Chai, W.S., Cheun, J.Y., Kumar, P.S., Mubashir, M., Majeed, Z., Banat, F., Ho, S.H., Show, P.L., 2021. A review on conventional and novel materials towards heavy metal adsorption in wastewater treatment application. J. Clean. Prod. 296, 126589 https://doi.org/10.1016/J.JCLEPRO.2021.126589.

Chowdhary, P., Bharagava, R.N., Mishra, S., Khan, N., 2020. Role of Industries in water scarcity and its adverse effects on environment and human health. Environ. Concerns Sustain. Dev. 235–256 https://doi.org/10.1007/978-981-13-5889-0_12.

Dharupaneedi, S.P., Nataraj, S.K., Nadagouda, M., Reddy, K.R., Shukla, S.S., Aminabhavi, T.M., 2019. Membrane-based separation of potential emerging pollutants. Sep. Purif. Technol. 210, 850–866. https://doi.org/10.1016/J.SEPPUR.2018.09.003.

Du, K., Cheng, Y., Yao, X., 2021. Environmental regulation, green technology innovation, and industrial structure upgrading: The road to the green transformation of Chinese cities. Energy Econ. 98, 105247 https://doi.org/10.1016/J.ENECO.2021.105247.

Dutta, D., Arya, S., Kumar, S., 2021. Industrial wastewater treatment: Current trends, bottlenecks, and best practices. Chemosphere 285, 131245. https://doi.org/10.1016/J.CHEMOSPHERE.2021.131245.

El-Sayed, M.Y., Alsohaimi, I.H., Alrashidi, A.N., Aldawsari, A.M., Alshahrani, A.A., Hassan, H.M.A., 2023. Mixed matrix membrane comprising functionalized sulfonated activated carbon from tea waste biomass for enhanced hydrophilicity and antifouling properties. Diam. Relat. Mater. 136, 109945 https://doi.org/10.1016/j.diamond.2023.109945.

Gassem, L. Ben, 2021. Saudi Arabia meeting water scarcity challenge with innovation [WWW Document]. Arab News. URL https://www.arabnews.com/node/1797816/business-economy.

Gong, Y., Gao, S., Tian, Y., Zhu, Y., Fang, W., Wang, Z., Jin, J., 2020. Thin-film nanocomposite nanofiltration membrane with an ultrathin polyamide/UIO-66-NH2 active layer for high-performance desalination. J. Memb. Sci. 600, 117874 https://doi.org/10.1016/j.memsci.2020.117874.

Hiratsuka, T., Tanaka, H., Miyahara, M.T., 2017. Mechanism of kinetically controlled capillary condensation in nanopores: A combined experimental and Monte Carlo approach. ACS Nano 11, 269–276. https://doi.org/10.1021/ACSNANO.6B05550.

Jeong, B.-H., Hoek, E.M.V., Yan, Y., Subramani, A., Huang, X., Hurwitz, G., Ghosh, A.K., Jawor, A., 2007. Interfacial polymerization of thin film nanocomposites: A new concept for reverse osmosis membranes. J. Memb. Sci. 294, 1–7. https://doi.org/10.1016/j.memsci.2007.02.025.

Jillani, S.M.S., Baig, U., Waheed, A., Ansari, M.A., 2022. NH2-CuO-MCM-41 covalently cross-linked multipurpose membrane for applications in water treatment: Removal of hazardous pollutants from water, water desalination and anti-biofouling performance. Chemosphere 307, 135592. https://doi.org/10.1016/j.chemosphere.2022.135592.

Kacprzak, M., Neczaj, E., Fijałkowski, K., Grobelak, A., Grosser, A., Worwag, M., Rorat, A., Brattebo, H., Almås, Å., Singh, B.R., 2017. Sewage sludge disposal strategies for sustainable development. Environ. Res. 156, 39–46. https://doi.org/10.1016/J.ENVRES.2017.03.010.

Kanesato, M., Yokoyama, T., Itabashi, O., Suzuki, T.M., Shiro, M., 1996. Synthesis and structural characterization of Praseodymium(III) and Neodymium(III) complexes of tripodal Tris[2-(salicylideneamino)ethyl]amine. Bull. Chem. Soc. Jpn 69, 1297–1302. https://doi.org/10.1246/bcsj.69.1297.

Kebria, M.R.S., Jahanshahi, M., Rahimpour, A., 2015. SiO 2 modified polyethyleneimine-based nanofiltration membranes for dye removal from aqueous and organic solutions. Desalination 367, 255–264. https://doi.org/10.1016/j.desal.2015.04.017.

Kumar Trivedi, M., Mohan Tallapragada, R., Branton, A., Trivedi, D., Nayak, G., Latiyal, O., Jana, S., 2015. Effect of Biofield Energy Treatment on Physical and Structural Properties of Calcium Carbide and Praseodymium Oxide. http://www.sciencepublishinggroup.com 4, 390. https://doi.org/10.11648/J.IJMSA.20150406.14.

Liu, H., Gao, J., Liu, G., Zhang, M., Jiang, Y., 2019. Enhancing permeability of thin film nanocomposite membranes via covalent linking of polyamide with the incorporated metal-organic frameworks. Ind. Eng. Chem. Res. 58, 8772–8783. https://doi.org/10.1021/acs.iecr.9b00772.

Ni, T., Ge, Q., 2018. Highly hydrophilic thin-film composition forward osmosis (FO) membranes functionalized with aniline sulfonate/bisulfonate for desalination. J. Memb. Sci. 564, 732–741. https://doi.org/10.1016/J.MEMSCI.2018.07.046.

Pang, R., Zhang, K., 2017. High-flux polyamide reverse osmosis membranes by surface grafting 4-(2-hydroxyethyl)morpholine. RSC Adv. 7, 40705–40710. https://doi.org/10.1039/C7RA06486A.

Qasem, N.A.A., Mohammed, R.H., Lawal, D.U., 2021. Removal of heavy metal ions from wastewater: a comprehensive and critical review. npj Clean. Water 4, 36. https://doi.org/10.1038/s41545-021-00127-0.

Rahimi, Z., Zinatizadeh, A.A., Zinadini, S., van Loosdrecht, M., Younesi, H., 2021. A new anti-fouling polysulphone nanofiltration membrane blended by amine-functionalized MCM-41 for post treating waste stabilization pond's effluent. J. Environ. Manage. 290, 112649 https://doi.org/10.1016/j.jenvman.2021.112649.

Saravanan, A., Senthil Kumar, P., Jeevanantham, S., Karishma, S., Tajsabreen, B., Yaashikaa, P.R., Reshma, B., 2021. Effective water/wastewater treatment

methodologies for toxic pollutants removal: Processes and applications towards sustainable development. Chemosphere 280, 130595. https://doi.org/10.1016/J.CHEMOSPHERE.2021.130595.

Saxena, A., Tripathi, B.P., Kumar, M., Shahi, V.K., 2009. Membrane-based techniques for the separation and purification of proteins: An overview. Adv. Colloid Interface Sci. 145, 1–22. https://doi.org/10.1016/J.CIS.2008.07.004.

Schleifer, L., 2017. 7 Reasons We're Facing a Global Water Crisis [WWW Document]. World Resour. Inst. URL https://www.wri.org/insights/7-reasons-were-facing-global-water-crisis.

Tahmasbi, B., Nikoorazm, M., Moradi, P., Tyula, Y.A., 2022. A Schiff base complex of lanthanum on modified MCM-41 as a reusable nanocatalyst in the homoselective synthesis of 5-substituted 1H-tetrazoles †. https://doi.org/10.1039/d2ra05413b.

Trisunaryanti, W., Larasati, S., Triyono, T., Santoso, N.R., Paramesti, C., 2020. Selective production of green hydrocarbons from the hydrotreatment of waste coconut oil over Ni- and NiMo-supported on amine-functionalized mesoporous silica. Bull. Chem. React. Eng. Catal. 15, 415–431. https://doi.org/10.9767/BCREC.15.2.7136.415-431.

Vshivkova, A.I., Gorelov, V.P., Kuz'Min, A. V., Plaksin, S. V., Pankratov, A.A., Yaroslavtseva, T. V., 2015. Preparation and physicochemical properties of praseodymium oxide films and ceramics. Inorg. Mater. 51, 1168–1176. https://doi.org/10.1134/S0020168515100179/METRICS.

Waheed, A., Baig, U., Aljundi, I.H., 2023a. Fabrication of polyamide thin film composite membranes using aliphatic tetra-amines and terephthaloyl chloride crosslinker for organic solvent nanofiltration. Sci. Rep. 13, 11691. https://doi.org/10.1038/s41598-023-38269-5.

Waheed, A., Baig, U., Jillani, S.M.S., 2023b. Optimization of amine functionalization of MCM-41 for its covalent decoration in nanofiltration membranes for purification of saline- and micropollutant-contaminated feeds. Environ. Sci.: Water Res. Technol. 9, 1371–1384. https://doi.org/10.1039/D2EW00883A.

Wang, Z., Chen, C., Liu, H., Hrynshpan, D., Savitskaya, T., Chen, J., Chen, J., 2020. Enhanced denitrification performance of Alcaligenes sp. TB by Pd stimulating to produce membrane adaptation mechanism coupled with nanoscale zero-valent iron. Sci. Total Environ. 708, 135063 https://doi.org/10.1016/j.scitotenv.2019.135063.

Wang, Z., Dai, L., Yao, J., Guo, T., Hrynsphan, D., Tatsiana, S., Chen, J., 2021. Enhanced adsorption and reduction performance of nitrate by Fe–Pd–Fe3O4 embedded multi-walled carbon nanotubes. Chemosphere 281, 130718. https://doi.org/10.1016/j.chemosphere.2021.130718.

Wang, Z., Hu, L., Zhao, M., Dai, L., Hrynsphan, D., Tatsiana, S., Chen, J., 2022. Bamboo charcoal fused with polyurethane foam for efficiently removing organic solvents from wastewater: experimental and simulation. Biochar 4, 28. https://doi.org/10.1007/s42773-022-00153-2.

Wang, J.J., Yang, H.C., Wu, M.B., Zhang, X., Xu, Z.K., 2017. Nanofiltration membranes with cellulose nanocrystals as an interlayer for unprecedented performance. J. Mater. Chem. A 5, 16289–16295. https://doi.org/10.1039/C7TA00501F.

Yadav, D., Karki, S., Ingole, P.G., 2022. Current advances and opportunities in the development of nanofiltration (NF) membranes in the area of wastewater treatment, water desalination, biotechnological and pharmaceutical applications. J. Environ. Chem. Eng. 10, 108109 https://doi.org/10.1016/j.jece.2022.108109.

Yu, L., Han, M., He, F., 2017. A review of treating oily wastewater. Arab. J. Chem. 10, S1913–S1922. https://doi.org/10.1016/J.ARABJC.2013.07.020.

Yung, L., Ma, H., Wang, X., Yoon, K., Wang, R., Hsiao, B.S., Chu, B., 2010. Fabrication of thin-film nanofibrous composite membranes by interfacial polymerization using ionic liquids as additives. J. Memb. Sci. 365, 52–58. https://doi.org/10.1016/J.MEMSCI.2010.08.033.

Zamani, H.A., Ganjali, M.R., Norouzi, P., Meghdadi, S., 2008. Application of Novel Praseodymium (III) PVC-Membrane Electrode for Determination of Pr(III) Ions in Soil and Sediment Samples. https://doi.org/10.1080/00032710801934957 41, 902–916. https://doi.org/10.1080/00032710801934957.